Efficient Seismic Source Localization Using Simplified Gaussian Beam Time Reversal Imaging

Fangyu Li, Tong Bai, Nori Nakata, Bin Lyu, and WenZhan Song, *Senior Member, IEEE*

***Abstract*— With the dramatic growth of seismic data volume, efficient and accurate seismic source location has become a significant challenge to seismologists. Recently, time reversal imaging (TRI) has been widely applied in automatic seismic source location for its robustness and accuracy, but its wave-equation-based implementation is usually computationally expensive. To achieve an efficient *in situ* and real-time source location, the emerging sensor network is a good option. In this article, we propose a simplified Gaussian beam TRI (SGTRI) method to implement the seismic source location in a distributed sensor network. Gaussian beam (GB) is a high-frequency asymptotic solution of the wave equation, which can help reduce the computation costs of the wavefield extrapolation in conventional TRI. Traditionally, the GB construction for reflection seismic imaging covers the entire subsurface space. However, for certain source localization, only limited areas contribute. Thus, we propose a beamforming-technique-based simplified GB construction to further boost efficiency. Then, we propose an imaging condition for the SGTRI to construct the final source location map. Using synthetic experiments, we demonstrate the accuracy, robustness, and efficiency of the proposed method compared with conventional TRI. In the end, a field application also shows promising results.**

***Index Terms*— Beamforming, distributed, Gaussian beam (GB), seismic source location, time reversal imaging (TRI).**

I. Introduction

SEISMIC source properties are important for analyzing natural and human activities, including earthquakes [1], geysers [2], volcanic activities [3], and human activities [4]. Thus, accurate, robust, and efficient seismic source location methods always draw researchers' attentions [5].

Manuscript received June 7, 2019; revised November 21, 2019; accepted January 2, 2020. This work was supported in part by the NSF under Grant 1663709 and in part by Southern Company. *(Corresponding author: Fangyu Li.)*

Fangyu Li and WenZhan Song are with the Center for Cyber-Physical Systems, University of Georgia, Athens, GA 30602 USA (e-mail: fangyu.li@uga.edu; wsong@uga.edu).

Tong Bai is with the Department of Geoscience, University of Wisconsin–Madison, Madison, WI 53706 USA (e-mail: tbai4@wisc.edu).

Nori Nakata is with the Department of Earth, Atmospheric and Planetary Sciences (EAPS), Massachusetts Institute of Technology (MIT), Cambridge, MA 02139 USA (e-mail: nnakata@mit.edu).

Bin Lyu is with the School of Geology and Geophysics, The University of Oklahoma, Norman, OK 73019 USA (e-mail: bin.lyu@ou.edu).

Color versions of one or more of the figures in this article are available online at http://ieeexplore.ieee.org.

Digital Object Identifier 10.1109/TGRS.2020.2964744

Recently, time reversal imaging (TRI) becomes popular in passive source location using seismic data [6]–[10], as well as borehole radar [11], ground-penetrating radar (GPR) [12], and ultrawideband (UWB) antenna array [13]. Compared with other methods based on arrival time difference [14], cross correlation [15], range difference [16], double time difference [17], and so on, TRI is advantageous as it is free of arrival-picking [18], which is usually the major factor for introducing uncertainties. TRI has been applied on low signal-to-noise ratio (SNR) data such as microseismic records or earthquake data, where the arrival times are not easy to pick [7].

Conventional TRI uses a finite-difference time domain (FDTD) algorithm to solve the wave equation [12], which has high computational cost due to the large iteration times of discrete wave equation calculation and the complexity of constructing absorbing boundary condition [19]. In addition, FDTD is sensitive to velocity errors because all wave equation-based wavefield reconstruction methods depend on a sufficiently accurate wavefield. Gaussian beam migration (GBM) is based on high-frequency approximation of wave equations [20], [21]. Because Gaussian beam (GB) is less influenced by the complex structure of velocity model [22], it has been applied in seismic source localization [23], [24]. Although GBM's accuracy is not as good as that of FDTD-based TRI, GB-based methods have obvious advantages in computation efficiency. In addition, for the source location purpose, only the wave propagation paths from receivers to sources need to be considered. Thus, a small portion of wavefield computation suffices.

Nowadays, to efficiently obtain *in situ* and real-time seismic imaging results, advanced wireless sensor networks with distributed computing algorithms have been utilized [5], [25]–[28]. For example, to monitor live volcano activities, wireless sensors were deployed using an air-dropped way [29]. In addition, the possibility of implementing TRI in a distributed sensor network has been investigated [30]. Fig. 1 shows a schematic example of a seismic source location based on TRI using a distributed sensor network.

In this article, we propose a simplified Gaussian beam TRI (SGTRI) algorithm to locate seismic sources. The proposed algorithm combines the efficiency of GB and the robustness of TRI. To further improve the efficiency to construct GBs with less computational resources, we apply the beamforming

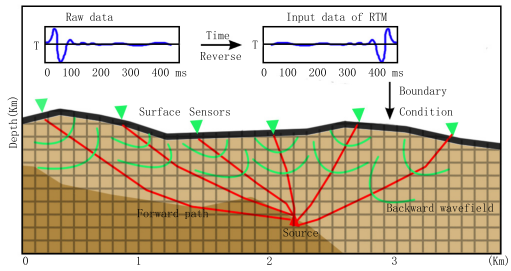

Fig. 1. TRI-based seismic source location.

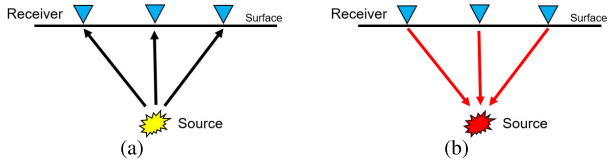

Fig. 2. Schematic plots of TRI source location. (a) Seismic wave forward propagation from a source to receivers. (b) Procedure of the TRI source location method, which back propagates the recorded data from receivers simultaneously into the subsurface and searches for a focusing point.

technique, which is an efficient direction of arrival (DOA) estimation method [31]. Simplified seismic wave propagation paths from sources to receivers are obtained, which take limited portions of the entire wavefield. We present synthetic and field experiments to validate the robustness, accuracy, computation/communication efficiency of our algorithm.

The contributions and innovations of this article are as follows.

1) We combine GB and TRI in the seismic source location. The innovative design takes advantages of both approaches and achieves accuracy and efficiency at the same time.
2) We propose to use a simplified beamforming-based GB construction and a distributed imaging condition to further improve the efficiency for the implementation in a sensor network, which can achieve *in situ* computing.
3) We propose a novel distributed seismic source location mechanism, which is tested through synthetic and field applications, showing promising results in terms of efficiency, robustness, and accuracy.

The remainder of this article is organized as follows. In Section II, we introduce the theoretical principles of TRI, GB construction, beamforming technique, and imaging condition. In Section III, we describe the proposed SGTRI algorithm in detail. Using the synthetic examples in Section IV, we analyze the image quality, robustness, and computation/communication complexity of our algorithm, compared with conventional algorithms. Later, a field application example is shown in Section V. Finally, conclusions are drawn in Section VI.

II. Theory

A. TRI for Seismic Source Location

The data $d(\mathbf{x}_r, \mathbf{x}_s, t)$ are recorded at a receiver located at $\mathbf{x}_r$, where $\mathbf{x}$ is the space coordinate. t is in the range $[0, T]$

$$d(\mathbf{x}_r, \mathbf{x}_s, t) = G(\mathbf{x}_r, \mathbf{x}_s, t) * S(t) \tag{1}$$

where $S(t)$ is a source, $G(\mathbf{x}_r, \mathbf{x}_s, t)$ denotes the Green's function which represents an impulse response observed at a receiver $\mathbf{x}_r$ due to a source at $\mathbf{x}_s$, and the symbol '*' represents the convolution operator.

The principle of TRI states that wavefields backward propagating in time from receivers focus at the source locations, as shown in Fig. 2. It consists of three steps: 1) reversing the recorded data in time; 2) backward-propagating the time-reversed data; and 3) applying the focusing imaging condition.

The backward propagation of recorded seismic data $d(\mathbf{x}_r, t)$ can be written as

$$W_d(\mathbf{x}, t) = G(\mathbf{x}, \mathbf{x}_r, t) * d(\mathbf{x}_r, T - t). \tag{2}$$

Thus, the seismic source location map can be obtained by

$$I_{\text{TRI}}(\mathbf{x}) = \|W_d(\mathbf{x}, t)\|_{IC} \tag{3}$$

where $\|\cdot\|_{IC}$ denotes the focusing imaging condition, e.g., maximum amplitude. Various imaging conditions can be used to obtain the source image $I_{\text{TRI}}(\mathbf{x})$ [7], [30], [32].

B. GB Construction

A GB is the high-frequency asymptotic solution to the wave equation in the ray centered coordinate system. We decompose Green's function by GBs

$$G_{\text{GB}}(\mathbf{x}', \mathbf{x}, t) = \int_0^{\pi} d\theta \int_0^{2\pi} d\phi \Phi(\theta, \phi, t) u_{\text{GB}}(\mathbf{x}', \mathbf{x}, \theta, \phi, t) \tag{4}$$

where $G_{\text{GB}}(\mathbf{x}', \mathbf{x}, t)$ represents Green's function constructed by summing GB wavefield $u_{\text{GB}}(\mathbf{x}', \mathbf{x}, \theta, \phi, t)$ from the source point $\mathbf{x}$ to field point $\mathbf{x}'$ with the central-ray takeoff angles θ and ϕ; $\Phi(\theta, \phi, t)$ is the initial amplitude factor for weighting the GBs to match the wavefield in the vicinity of the source location.

In the ray-centered coordinate system, the GB wavefield can be expressed as [20]

$$u_{\text{GB}}(\mathbf{x}', \mathbf{x}, \theta, \phi, t) = u_{\text{GB}}(s, q_1, q_2, \mathbf{x}, \mathbf{p}, t) \tag{5}$$

where s is the distance along the raypath; q_1 and q_2 represent the two perpendicular distances from the raypath in the local ray-centered coordinates to the field point; $\mathbf{p} = (p_x, p_y, p_z)$ is the ray parameter vector. The details of the formula and the choice of the initial parameters for GBs, such as initial beamwidth, beam center interval, ray takeoff angle interval, and weighting factor can be readily found in the literature [20].

C. Simplified GB Construction Based on Beamforming

GB is based on ray-tracing, which is computationally more efficient than wave equation methods but can be still expensive. As shown in Fig. 3, we propose to use beamforming to initialize the directions of GBs, and relatively wide GBs are constructed to ensure the source is within the beam ranges.

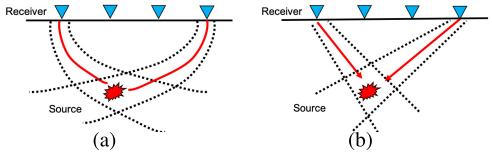

Fig. 3. Schematic plots of (a) GB-based and (b) simplified GB-based source location. In (a) GBs are constructed based on the ray tracing, while in (b) GB centers are obtained by beamforming, which simplifies GB constructions and saves computations. Red curves: GB centers. Black dashed curves: GB ranges.

Given a set of M sensors, with location coordinates $[(x_0, y_0), (x_1, y_1), \ldots, (x_{m-1}, y_{m-1})]^T$, the array response vector or the steering vector $a(f)$ can be expressed as [31]

$$a(f) = [e^{-i2\pi f \tau_0}, e^{-i2\pi f \tau_1}, \ldots, e^{-i2\pi f \tau_{m-1}}] \tag{6}$$

where $\tau_m = x_m p \cos\varphi + y_m p \sin\varphi$ is the time delay for signal to reach the mth sensor from the origin, and p, φ are the slowness and the angle of propagation, respectively.

A frequency-domain beamforming method is implemented to estimate the phase velocities and directions of propagation. Conventional beamforming methods make use of the data covariance matrix to obtain the power associated with a steering vector [33]. In the time domain, it can be interpreted as a simple method of delay and sum. The power of the stacked signal provides information about the accuracy of the delay applied. The beampower BP(f) corresponding to a steering vector $a_k(f)$ is computed as

$$BP(f) = a_k^*(f) R_{xx}(f) a_k(f) \tag{7}$$

where $*$ represents the complex conjugate, $R_{xx} = X(f)X^*(f)$ is the frequency domain data covariance matrix. The largest obtained BP indicates the wave propagation direction φ.

D. Source Imaging Condition

Using the simplified GB (SGB) construction in Sections II-B and II-C, the SGTRI backward propagation from a single sensor node r can be written as

$$W_{d,r}^{\mathrm{SGB}}(\mathbf{x}, \mathbf{t}) = u_{\mathrm{SGB}}(\mathbf{x}, \mathbf{x}_r, t) * d(\mathbf{x}_r, T - t). \tag{8}$$

Then, combining wavefields generated from all sensor nodes in the network, the source location map can be expressed as

$$I_{\mathrm{SGTRI}}(\mathbf{x}) = \left\| W_{d,r}^{\mathrm{SGB}}(\mathbf{x}, \mathbf{t}) \right\|_{IC}. \tag{9}$$

To generate the source location image, the stacked/cross correlation imaging condition [30] and geometric mean imaging condition [7] have been proposed. Here, we propose a novel imaging condition designed for distributed sensor networks

$$I_{\mathrm{SGTRI}}(\mathbf{x}) = \sum_K \sum_T \prod_M W_{d,r}^{\mathrm{SGB}}(\mathbf{x}, \mathbf{t}) \tag{10}$$

where the N receivers are divided into K clusters, and each cluster has M receivers, so $N = K \times M$. Note that it involves a two-level communication: first, the raw data in the same cluster are sent to the sink node[1]; second, the SGBs from different clusters will be transmitted over the network for the final imaging. Because SGBs cover smaller portion of subsurface than wavefield extrapolation methods, the computation and communication costs can be reduced.

[1]All the communication in a sensor network takes place between source and destination. The destination is called sink.

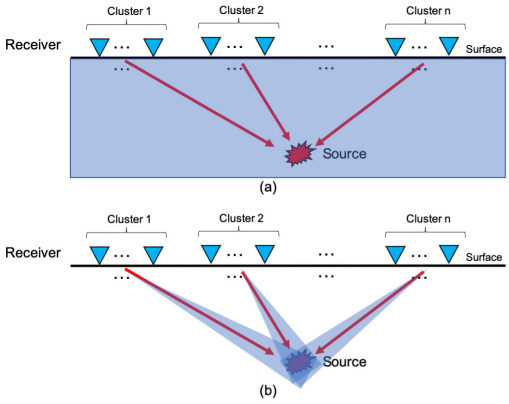

Fig. 4. Schematic plots of SGTRI-based source location. (a) Conventional TRI imaging condition proposed in [30] needs to calculate the wavefield extrapolation of the whole subsurface space. (b) SGTRI only computes the shadowed SGB areas, which save computations. Note that the source location is the position, where all wavefields coincide.

Fig. 4 shows the comparison between the conventional TRI imaging condition proposed in [30] and our SGTRI method. Instead of calculating the wave extrapolation in the entire space, only the SGB areas are used in our method, which reduces the computation significantly.

III. Algorithm

Compared with the conventional TRI shown in Fig. 1, SGTRI has the following differences: 1) backward propagated wavefields reconstructed by GB rather than, e.g., FDTD, which is often adopted in conventional TRI; 2) only the wave propagation trace area is considered and an even simplified solution is adopted; 3) the image condition is hierarchical with two levels; and 4) the absorbing boundary condition and the scattering effect of velocity model are avoided as a smooth velocity model is employed. Algorithm 1 describes the detailed steps of the proposed algorithm. In addition, the "multiple sources" situations can be inferred following [10] and [34].

Algorithm 1 Proposed SGTRI Algorithm

1: Locally cluster sensor nodes.
2: Data transmission to the sink node in the cluster.
3: Apply beamforming to initialize the GBs.
4: Construct the back-propagating wavefield within the GB range.
5: Transmit GBs among sink nodes from different clusters in the whole network.
6: Apply the proposed imaging condition to generate the source location energy map.
7: Pick the strong energy area as the source location result.

IV. Synthetic Experiments

The numerical experiment is implemented on Marmousi velocity model [35]. We selected a small area in Marmousi

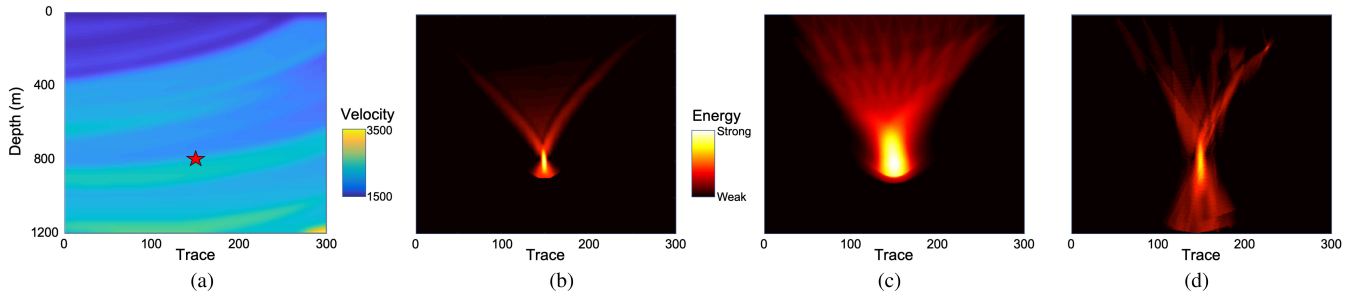

Fig. 5. Synthetic seismic source location example. (a) Velocity model with one seismic source located at (150, 800) with results from (b) TRI, (c) distributed TRI proposed in [10], and (d) proposed SGTRI.

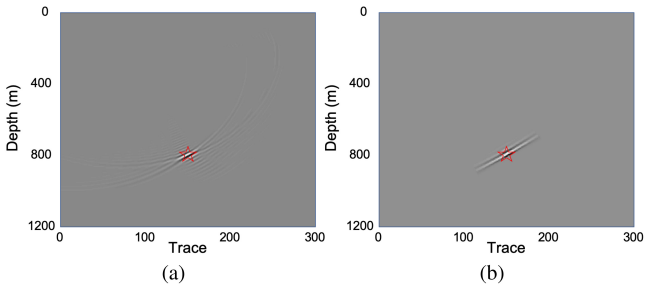

Fig. 6. Wavefields generated by (a) distributed TRI and (b) SGTRI from the first sensor cluster.

model which contains multiple layers, which is shown in Fig. 5(a). The velocity field ranges from 1500 to 3500 m/s. The size of the velocity model is 300×300, and the depth interval dz and width interval dx are both 4 m. The surface sensor array has the same deployment as the first test, which consists of 41 sensors with an interval of 30 m. Each node also receives raw data from six neighbors to initialize the directions of GBs. We set up a single seismic source at ($x = 600$ m, $z = 800$ m) with a time length of 0.6 s, and the time interval is 0.5 ms.

Fig. 5(b) shows the TRI imaging result, where we can easily find that the strong energy spot is on the true location of the seismic source. Fig. 5(c) displays the distributed TRI imaging result proposed in [10]. Although the solution saves communication costs, the resolution is significantly sacrificed. The proposed SGTRI method generates a satisfactory resolution comparable with that of conventional TRI. Despite a little more vertical smearing, the source location can be easily pointed out.

The snapshots in Fig. 6 benchmark the wavefield produced by SGTRI with that by TRI. It is clear that SGTRI calculates only limited areas, whereas TRI needs to cover the whole space, as the constructed wavefronts extrapolate widely in Fig. 6(a). Furthermore, GB-based wavefield construction is generally more efficient than FDTD-based TRI. Thus, SGTRI is much more efficient than TRI. In sum, SGTRI is an efficient tool for seismic source location with acceptable imaging quality.

The robustness of TRI methods has been discussed by previous researches [30], [34], [36], [37]. Here, we add different levels of random noises to test the robustness of

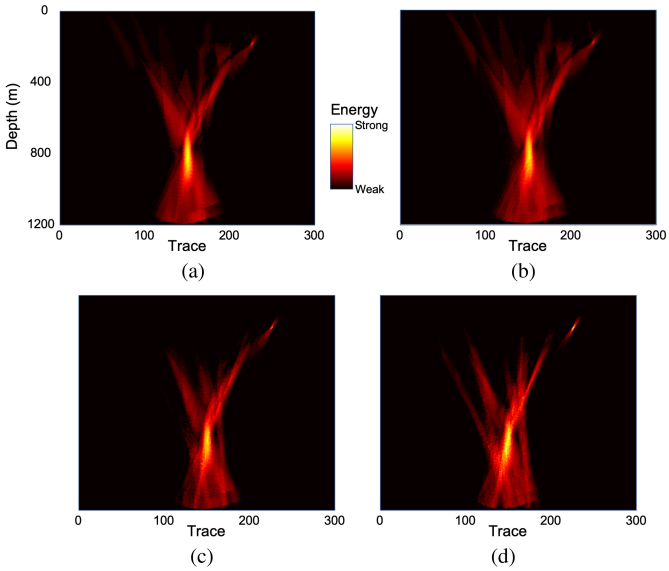

Fig. 7. Robustness tests of the proposed method with different SNRs. (a) 10 dB. (b) 0 dB. (c) -10 dB. (d) -20 dB.

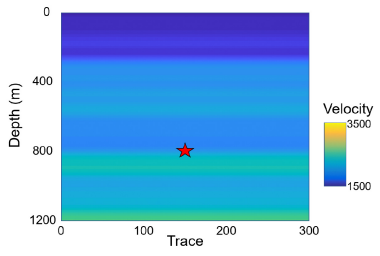

Fig. 8. 1-D seismic velocity model for testing the source location robustness to the velocity errors.

the proposed SGTRI method. Fig. 7 shows the final energy maps with different noise levels at SNR $= 10$, 0, -10, and -20 dB, respectively. It turns out that our proposed method is robust even under an extremely noisy (-20 dB) environment. Although low SNR may cause some unexpected artifacts, the energy focusing at the actual source location remains distinguishable from noise-induced artifacts.

To explore the tolerance of TRI and SGTRI to velocity errors, we compare their imaging results (see Fig. 9) using a 1-D velocity model in Fig. 8, which is extracted from the

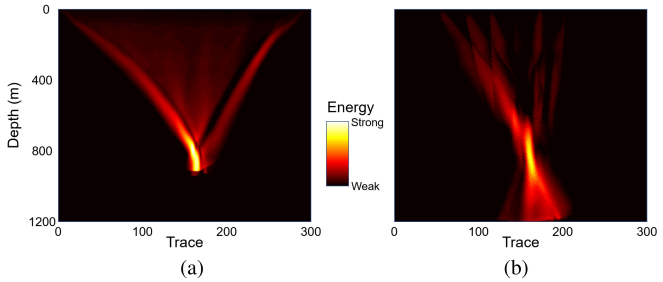

Fig. 9. Source location results based the 1-D velocity model in Fig. 8 using (a) TRI and (b) SGTRI.

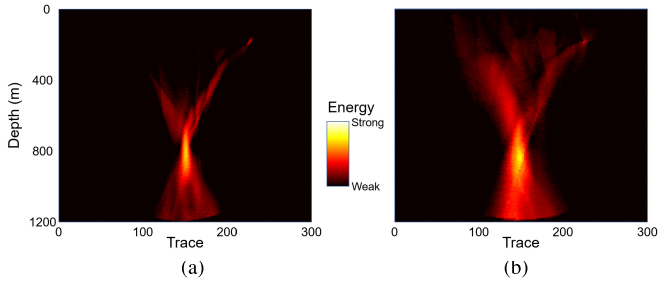

Fig. 10. Source location results based on SGTRI using different sensor numbers in the cluster. (a) 12. (b) 3.

central position in Fig. 5(a). Compared with results shown in Fig. 5, source location deviations of different methods caused by velocity errors vary. SGTRI generates amore consistent lateral location. In addition, the vertical resolution by TRI is severely deteriorated [comparing Fig. 9(a) with Fig. 5(b)] whereas it is preserved by SGTRI, demonstrating the less sensitivity of SGTRI to velocity errors.

Next, since SGTRI is designed for a distributed application, we investigate the influence of the number of traces in the cluster. Fig. 10 displays results using surrounding 12 [see Fig. 10(a)] and 3 [see Fig. 10(b)] neighboring traces. Compared with the original result using six neighboring traces shown in Fig. 5(d), more traces in a cluster produce higher energy concentration. However, even when based on a limited number of traces, the source location is still acceptable as Fig. 10(b).

We run all experiments using a computer with 8 cores CPU, 3.40 GHz, and 31.3-GB memory. Table I shows the computational cost of TRI and SGTRI. GB construction needs only ray parameters and raw data, whereas FDTD needs medium parameters of the whole velocity model and perfectly matched layers. The GB configuration is ten times faster than the FDTD method. The beamforming step is also efficient. Because the imaging condition of SGTRI defined in (3) is more complicated than TRI, the imaging computation time is a little longer. In general, SGTRI is significantly faster than TRI in computation, resulting in a potential real-time seismic imaging solution.

Table II shows the communication cost comparison. To generate the final imaging result, the backward wavefield should be sent to the whole network through broadcast, which is the most expensive part. The SGTRI calculates only the backward

TABLE I
COMPUTATION COST COMPARISON

	Algorithm	Memory(Mb)	Time(s)
TRI	Wavefield solving	920	9.098
	Imaging	100	0.072
SGTRI	Beamforming	330	0.468
	GB-based wavefield solving	440	0.836
	Imaging	100	0.325

TABLE II
COMMUNICATION COST COMPARISON

Algorithm		Broadcast volume(Mb)	Unicast volume(Mb)
TRI	Imaging	38400	0
SGTRI	Beamforming	0	15.4
	Imaging	5900	0

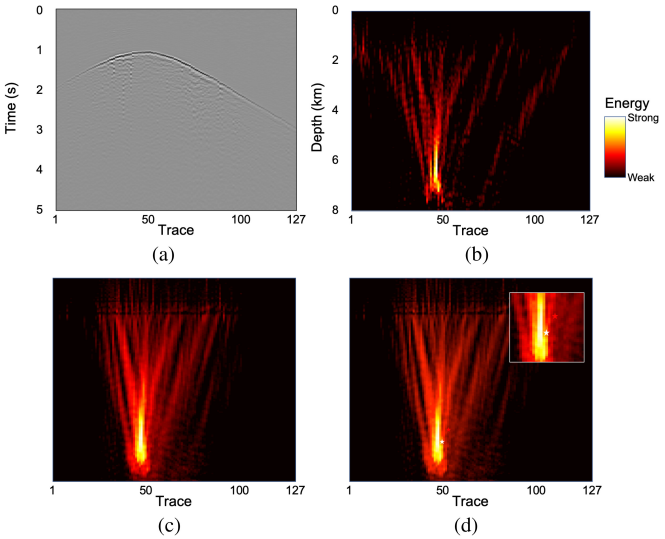

Fig. 11. (a) Field seismic data, which are filtered to $1 \sim 10$ Hz to highlight the signal and reduce high-frequency noise. Earthquake source location using (b) TRI method and (c) proposed SGTRI method. (d) Comparison with the location results from OGS (white star) and [38] (red star).

propagated wavefield in the range of one single GB, which is only one-tenth or even less area of the whole wavefield, as shown in Fig. 4. So SGTRI has less communication burdens in the imaging stage. In addition, only raw data are transmitted within each cluster, which is much smaller than wavefields used in TRI. It is obvious that the proposed method has advantages in saving both computation and communication costs.

V. FIELD EXPERIMENT

To further evaluate the proposed SGTRI method, we apply it to a field seismic data set. There was an $M2.3$ earthquake on July 11, 2016 in Enid, OK, USA, recorded by Incorporated Research Institutions for Seismology (IRIS).[2] Fig. 11(a) shows

[2]The seismic data available at http://ds.iris.edu/mda/YW?timewindow=2016-2016 (Last accessed June 7, 2019.)

the recorded waveforms from 127 geophones on one around 12-km-long seismic line in the east–west direction with a sampling interval of 4 ms. Using a 1-D velocity model from Oklahoma Geological Survey (OGS), we apply TRI and SGTRI to locate the earthquake source. The results are shown in Fig. 11(b) and (c), respectively. It is clear that although the resolution of SGTRI is little lower than that of TRI, the earthquake source locations are very close. Considering the computation and communication reduction, SGTRI has its own advantages in specific applications.

For further validation, the source location result[3] from OGS and a relocation result[4] from [38] using a modified velocity model are plotted in Fig. 11(d) for comparison. Our result is close to the reference location results. The minor discrepancy comes from the differences in seismic source location methods, velocity models, as well as data sets.[5] Thus, SGTRI has a comparable source localization accuracy with existing methods.

VI. Conclusion

In this article, we propose a seismic source location algorithm named SGTRI, which is developed for distributed sensor networks. The proposed method has advantages in computation and communication costs. Instead of FDTD, GB calculates the approximate solution of the wave equation and deals with the uncertain velocity model issue. Beamforming technique is used to construct simplified GBs. SGTRI also inherits the robustness of conventional TRI. With the theoretical derivations and results of numerical experiments, we can conclude that the SGTRI algorithm is suitable for a real-time distributed system because of its efficiency.

References

[1] B. Gutenberg, "Microseisms," in *Advances in Geophysics*, vol. 5. Amsterdam, The Netherlands: Elsevier, 1958, pp. 53–92.

[2] P. Jeanne, J. Rutqvist, C. Hartline, J. Garcia, P. F. Dobson, and M. Walters, "Reservoir structure and properties from geomechanical modeling and microseismicity analyses associated with an enhanced geothermal system at The Geysers, California," *Geothermics*, vol. 51, pp. 460–469, Jul. 2014.

[3] J.-P. Métaxian, P. Lesage, and J. Dorel, "Permanent tremor of Masaya Volcano, Nicaragua: Wave field analysis and source location," *J. Geophys. Res.*, vol. 102, no. B10, pp. 22529–22545, Oct. 1997.

[4] A. L. Liaw and T. McEvilly, "Microseisms in geothermal exploration—Studies in Grass Valley, Nevada," *Geophysics*, vol. 44, no. 6, pp. 1097–1115, 1979.

[5] W. Song, F. Li, M. Valero, and L. Zhao, "Toward creating a subsurface camera," *Sensors*, vol. 19, no. 2, p. 301, Jan. 2019.

[6] B. Artman, I. Podladtchikov, and B. Witten, "Source location using time-reverse imaging," *Geophys. Prospecting*, vol. 58, no. 5, pp. 861–873, Sep. 2010.

[7] N. Nakata and G. C. Beroza, "Reverse time migration for microseismic sources using the geometric mean as an imaging condition," *Geophysics*, vol. 81, no. 2, pp. KS51–KS60, Mar. 2016.

[8] B. Witten and J. Shragge, "Image-domain velocity inversion and event location for microseismic monitoring," *Geophysics*, vol. 82, no. 5, pp. KS71–KS83, Sep. 2017.

[9] B. Lyu, N. Nakata, and K. J. Marfurt, "A reverse time migration workflow of passive source with joint-imaging conditions," in *Proc. SEG Tech. Program Expanded Abstracts*, Aug. 2018, pp. 2947–2951.

[10] F. Li, Y. Qin, and W. Song, "Waveform inversion-assisted distributed reverse time migration for microseismic location," *IEEE J. Sel. Topics Appl. Earth Observ. Remote Sens.*, vol. 12, no. 4, pp. 1327–1332, Apr. 2019.

[11] H. Yang, T. Li, N. Li, Z. He, and Q. H. Liu, "Time-gating-based time reversal imaging for impulse borehole radar in layered media," *IEEE Trans. Geosci. Remote Sens.*, vol. 54, no. 5, pp. 2695–2705, May 2016.

[12] C. Leuschen and R. Plumb, "A matched-filter-based reverse-time migration algorithm for ground-penetrating radar data," *IEEE Trans. Geosci. Remote Sens.*, vol. 39, no. 5, pp. 929–936, May 2001.

[13] M. E. Yavuz and F. L. Teixeira, "Space–frequency ultrawideband time-reversal imaging," *IEEE Trans. Geosci. Remote Sens.*, vol. 46, no. 4, pp. 1115–1124, Apr. 2008.

[14] H. Schau and A. Robinson, "Passive source localization employing intersecting spherical surfaces from time-of-arrival differences," *IEEE Trans. Acoust., Speech, Signal Process.*, vol. 35, no. 8, pp. 1223–1225, Aug. 1987.

[15] Y. Huang, J. Benesty, G. Elko, and R. Mersereati, "Real-time passive source localization: A practical linear-correction least-squares approach," *IEEE Trans. Speech Audio Process.*, vol. 9, no. 8, pp. 943–956, Nov. 2001.

[16] J. Abel and J. Smith, "The spherical interpolation method for closed-form passive source localization using range difference measurements," in *Proc. IEEE Int. Conf. Acoust., Speech, Signal Process. (ICASSP)*, Mar. 2005, pp. 471–474.

[17] J. Qian, H. Zhang, and E. Westman, "New time-lapse seismic tomographic scheme based on double-difference tomography and its application in monitoring temporal velocity variations caused by underground coal mining," *Geophys. J. Int.*, vol. 215, no. 3, pp. 2093–2104, Dec. 2018.

[18] F. Li*, J. Rich, K. J. Marfurt, and H. Zhou, "Automatic event detection on noisy microseismograms," in *Proc. SEG Tech. Program Expanded Abstracts 2014*, Aug. 2014, pp. 2363–2367.

[19] P. Yang, J. Gao, and B. Wang, "RTM using effective boundary saving: A staggered grid GPU implementation," *Comput. Geosci.*, vol. 68, pp. 64–72, Jul. 2014.

[20] N. R. Hill, "Prestack Gaussian-beam depth migration," *Geophysics*, vol. 66, no. 4, pp. 1240–1250, Jul. 2001.

[21] S. Gu, C. Li, X. Gao, Z. Sun, and G. Fang, "Three-dimensional image reconstruction of targets under the illumination of terahertz Gaussian beam—Theory and experiment," *IEEE Trans. Geosci. Remote Sens.*, vol. 51, no. 4, pp. 2241–2249, Apr. 2013.

[22] U. Albertin, D. Yingst, P. Kitchenside, and V. Tcheverda, "True-amplitude beam migration," in *Proc. SEG Tech. Program Expanded Abstracts*, 2004, pp. 949–952.

[23] S. Rentsch, S. Buske, S. Lüth, and S. A. Shapiro, "Location of seismicity using Gaussian beam type migration," in *Proc. SEG Tech. Program Expanded Abstracts*, Jan. 2004, pp. 354–357.

[24] S. Rentsch, S. Buske, S. Lüth, and S. A. Shapiro, "Fast location of seismicity: A migration-type approach with application to hydraulic-fracturing data," *Geophysics*, vol. 72, no. 1, pp. S33–S40, Jan. 2007.

[25] M. Valero, F. Li, W. Song, and X. Li, "Imaging subsurface civil infrastructure with smart seismic network," in *Proc. IEEE 37th Int. Perform. Comput. Commun. Conf. (IPCCC)*, Nov. 2018, pp. 1–8.

[26] M. Valero, F. Li, S. Wang, F.-C. Lin, and W. Song, "Real-time cooperative analytics for ambient noise tomography in sensor networks," *IEEE Trans. Signal Inf. Process. Netw.*, vol. 5, no. 2, pp. 375–389, Jun. 2019.

[27] M. Valero, F. Li, J. Clemente, and W. Song, "Distributed and communication-efficient spatial auto-correlation subsurface imaging in sensor networks," *Sensors*, vol. 19, no. 11, p. 2427, May 2019.

[28] J. Clemente, F. Li, M. Valero, A. Chen, and W. Song, "ASIS: Autonomous seismic imaging system with *in situ* data analytics and renewable energy," *IEEE Syst. J.*, to be published.

[29] W.-Z. Song, R. Huang, M. Xu, A. Ma, B. Shirazi, and R. Lahusen, "Air-dropped sensor network for real-time high-fidelity volcano monitoring," in *Proc. 7th Int. Conf. Mobile Syst., Appl., Services (Mobisys)*, 2009, pp. 305–318.

[30] J. Sun, T. Zhu, S. Fomel, and W.-Z. Song, "Investigating the possibility of locating microseismic sources using distributed sensor networks," in *Proc. SEG Tech. Program Expanded Abstracts*, Aug. 2015, pp. 2485–2490.

[31] J. W. Woods and P. R. Lintz, "Plane waves at small arrays," *Geophysics*, vol. 38, no. 6, pp. 1023–1041, Dec. 1973.

[3] {*lat* 36.642439, *lon* -97.689520, *depth* 6560 m}

[4] {*lat* 36.615857, *lon* -97.686024, *depth* 6051 m}

[5] We use only a 2-D seismic line in this article, while OGS used available seismic data over Oklahoma, and additional Kansas data were also used in [38].

[32] T. Zhu and J. Sun, "Data-driven diffraction imaging of fractures using passive seismic data," in *Proc. SEG Tech. Program Expanded Abstracts*, Sep. 2016, pp. 2679–2683.
[33] D. H. Johnson and D. E. Dudgeon, *Array Signal Processing: Concepts and Techniques*. Englewood Cliffs, NJ, USA: Prentice-Hall, 1993.
[34] T. Zhu, J. Sun, D. Gei, J. M. Carcione, P. Cance, and C. Huang, "Hybrid multiplicative time-reversal imaging reveals the evolution of microseismic events: Theory and field-data tests," *Geophysics*, vol. 84, no. 3, pp. KS71–KS83, May 2019.
[35] R. Versteeg, "The Marmousi experience: Velocity model determination on a synthetic complex data set," *Lead. Edge*, vol. 13, no. 9, pp. 927–936, Sep. 1994.
[36] N. Nakata and G. C. Beroza, "Reverse-time migration for microseismic sources using the geometric mean as an imaging condition," in *Proc. SEG Tech. Program Expanded Abstracts*, Aug. 2015, pp. 2451–2455.
[37] T. Zhu, "Time-reverse modelling of acoustic wave propagation in attenuating media," *Geophys. J. Int.*, vol. 197, no. 1, pp. 483–494, Apr. 2014.
[38] M. Schoenball and W. L. Ellsworth, "Waveform-relocated earthquake catalog for Oklahoma and Southern Kansas illuminates the regional fault network," *Seismolog. Res. Lett.*, vol. 88, no. 5, pp. 1252–1258, Sep. 2017.

Fangyu Li received the bachelor's degree in electrical engineering from Tsinghua University, Beijing, China, the master's degree in electrical engineering from the Beihang University, Beijing, and the Ph.D. degree in geophysics from The University of Oklahoma, Norman, OK, USA, in 2017.

He is currently a Post-Doctoral Fellow with the College of Engineering, University of Georgia, Athens, GA, USA. His research interests include signal processing, inverse problems, seismic ambient noise imaging, time-reversal imaging (TRI), seismic source location, machine learning, distributed computing, and sensor networks.

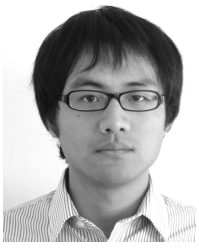

Tong Bai received the Ph.D. degree in geophysics from the Colorado School of Mines, Golden, CO, USA, in 2019.

He is currently a Post-Doctoral Research Associate with the Department of Geoscience, University of Wisconsin–Madison, Madison, WI, USA. His research interests include seismic wave propagation and imaging techniques in complex (anisotropic and viscoelastic) media, as well as inverse problems (travel time and waveform tomography, and ambient noise surface wave tomography).

Nori Nakata received the Bachelor of Engineering and Master of Engineering degrees from Kyoto University, Kyoto, Japan, in 2008 and 2010, respectively, and the Ph.D. degree from the Colorado School of Mines, Golden, CO, USA, in 2013.

He is currently a Principal Research Scientist with the Department of Earth, Atmospheric and Planetary Sciences, Massachusetts Institute of Technology (MIT), Cambridge, MA, USA. Before he joined MIT in 2019, he was a Post-Doctoral Fellow with the Stanford University, Stanford, CA, USA, from 2013 to 2016, and an Assistant Professor with The University of Oklahoma, Norman, OK, USA, from 2016 to 2018. His research interests are extensive and include crustal/global seismology, exploration geophysics, volcanism, civil engineering, wave phenomena, and earthquakes.

Dr. Nakata received the Mendenhall Prize from the Colorado School of Mines for his Ph.D.

Bin Lyu received the B.S. and M.S. degrees in geophysics from the China University of Petroleum, Beijing, China, in 2003 and 2006, respectively. He is currently pursuing the Ph.D. degree in geophysics with The University of Oklahoma, Norman, OK, USA, as a Graduate Research Assistant of the AASPI Consortium.

From 2006 to 2015, he was a Processing Geophysicist with the Petrochina Research Institute of Petroleum Exploration and Development-Northwest, Lanzhou, Gansu, China. His research interests include new seismic attributes development and interpretation, seismic processing, reverse-time migration (RTM), full-waveform inversion (FWI), passive seismic imaging, and seismic anisotropy.

WenZhan Song (Senior Member, IEEE) received the B.S. and M.S. degrees from the Nanjing University of Science and Technology, Nanjing, China, in 1997 and 1999, and the Ph.D. degree in computer science from the Illinois Institute of Technology, Chicago, IL, USA, in 2005.

He is currently a Chair Professor of electrical and computer engineering with the University of Georgia, Athens, GA, USA. His research focuses on cyber-physical systems and their applications in energy, environment, food, and health sectors.

Dr. Song received the NSF CAREER Award in 2010.